KRONOS FUSION ENERGY

PAPER 2.31 · THE KRONOS 2026 SERIES

Beryllium and $Be_{12}Ti$ Neutron Multipliers for a Compact Spherical-Tokamak Breeder: Pebble Performance, Activation, and Closing Net TBR ≥ 1.05

Tritium self-sufficiency in a compact deuterium–tritium breeder is bought by the neutron multiplier, and the choice of multiplier material and its pebble-bed form are the levers...

Read it live — 3-D model · physics validator · film series

BY P I FORD AND G L KULCINSKI

2026 · EDITORIAL EDITION

THE OFFICIAL RECORD

What this document is, and how to read its numbers

This is a combined editorial. It gathers, in one volume, the two design studies Kronos Fusion Energy released in 2026 — a compact spherical-tokamak tritium/helium-3 breeder and a deuterium–helium-3 tandem-mirror generator — together with the intellectual-property estate, the people, and, in the internal edition, the full commercial case. The scientific text is the same text that appears in the arXiv preprints and the journal submissions; the editorial adds the apparatus a reader needs to hold the whole program at once, and nothing in the physics is altered to fit it.

THE HONESTY STANCE IS THE ASSET

Every headline quantity carries an **evidence class** — DERIVED RECOMPUTED MEASURED REQUIREMENT — and, where a number is a modelled extrapolation rather than a demonstrated value, it is labelled as such and its downside is shown next to it. Several quantities in the underlying corpus moved after first publication; where a value has been withdrawn or restated, the record says so plainly. This is deliberate: a diligence team will find the load-bearing assumptions, so the document surfaces them first.

TWO EDITIONS

This volume is issued in two editions. The **public edition** (light) carries the physics and the design only — no dollar, price, or per-kilogram figure appears anywhere in it. The **internal edition** (dark) adds the economics, the funding architecture, and the defense-commercial analysis, and is marked *Confidential* accordingly; it is not for public distribution. Where the commercial case rests on a modelled assumption rather than a demonstrated one, it is labelled as such and its downside is shown alongside it, on the same terms as the physics.

TITLE	The Kronos Fleet — Hyperion · Aegis · MetroVolt: A Combined Design & Commercialization Study
AUTHOR	Priyanca Ford, Founder & CEO, on behalf of Kronos Fusion Energy
EDITION	2026 Combined Editorial · first issue
COMPANION WORKS	The five-paper arXiv drop — (1) Breeder, (2) Burner, (3) REBCO magnet & tape, (4) Direct Energy Conversion, (5) AI/ML/Quantum control — with matching numbered Zenodo deposits, plus the IOP journal and IAEA-FEC submissions. Patents were filed before the drop.
NAMING	Hyperion = the breeder; Aegis (defense) and MetroVolt (data-center) = one generator in two housings. Internal mode letters (D1, L) do not appear on public surfaces.
STATUS	Conceptual design & simulation study. Nothing herein is a construction commitment.

HOW TO READ THIS VOLUME

The fleet at a glance, and the way its numbers are marked

This volume opens with *Orientation*, presents the five research papers as a bound sequence, and closes with the *Apparatus*. *Foundations* sets out the three general results both machines rest on. *Paper One* is the Hyperion breeder; *Paper Two* the Aegis / MetroVolt generator; *Papers Three, Four and Five* are the enabling science — high-field REBCO magnets and tape, direct energy conversion, and the AI / ML / quantum control stack. A *Digital Twin & 3-D Model* part follows, then the *Environmental* profile. The *Economics* and levelized cost and the *Business Case* and diligence record appear in the internal edition only; the *Simulations* proof record and the Apparatus — patent portfolio, team, limitations, and sources — close both editions.

THE FLEET AT A GLANCE

	HYPERION	AEGIS	METROVOLT
Role	Strategic-isotope foundry	Defense installation power	Campus power
Machine	**Spherical tokamak**	**Tandem mirror**	**Tandem mirror**
Fuel	Deuterium–tritium	Deuterium–helium-3	Deuterium–helium-3
Delivers	Tritium · ^{3}He · 14 MeV n	Resilient installation power	Firm campus power
Physics bar	**Fusion gain only**	Closure (gates named)	Closure + lunar ^{3}He
In the fleet	Breeds the fuel	Proves the generator	Commercial destination

HOW THE NUMBERS ARE MARKED

Every headline quantity carries an evidence class — DERIVED from first principles, RECOMPUTED from raw data, MEASURED in hardware, or a REQUIREMENT yet to be met. Financial figures carry a case label and are confined to the internal (confidential) edition. Values that moved after first publication are shown as withdrawn or restated rather than quietly changed. A capability you can evaluate is one whose limits are on the page.

ABSTRACT

Beryllium and $Be_{12}Ti$ Neutron Multipliers for a Compact Spherical-Tokamak Breeder: Pebble Performance, Activation, and Closing Net TBR ≥ 1.05

Tritium self-sufficiency in a compact deuterium–tritium breeder is bought by the neutron multiplier, and the choice of multiplier material and its pebble-bed form are the levers that decide whether the blanket breaks even. We qualify the multiplier for the Kronos *Hyperion* spherical-tokamak breeder ($P_{\text{fus}} = 85.04\,\text{MW}$, $Q = 3.076$, $I_p = 9.66\,\text{MA}$, $R_0 = 1.20\,\text{m}$, aspect ratio $A = 2.5$, $B_0 = 8\,\text{T}$) by solving the steady-state linear Boltzmann transport equation over the closing blanket configuration in coupled continuous-energy Monte Carlo and swapping only the breeder-zone multiplier material. We formalise the tritium-breeding ratio (TBR) as a reaction-rate functional of the neutron flux, decompose the neutron-multiplication factor into its threshold $(n, 2n)$ and $(n, 3n)$ channels, and derive the net-TBR self-sufficiency condition $\Lambda = \text{TBR}\,(1 - \varepsilon) - 1 \geq 0$ together with the inventory-doubling time it implies. Beryllium is confirmed the best multiplier, closing at **net TBR** 1.054 ± 0.001; the beryllide $\mathrm{Be_{12}Ti}$ is the only credible alternative, holding self-sufficiency at a razor-thin 1.002 ± 0.001 while answering beryllium's helium-swelling problem. Every lead-bearing and molten-salt option falls below closure — FLiBe 0.908, PbLi 0.828, lead pebble 0.806. The verdict is library-robust: FENDL-3.2 and ENDF/B-VIII.0 agree to 0.5–$0.6\,\%$, far inside the gap to closure. In its blanket the beryllium multiplier lifts the breeding ratio from an as-drawn 0.742 deficit to the canonical 1.189, clearing the 1.05 self-sufficiency gate with margin and held below the 1.42 design ceiling. Activation is dominated by prompt $^{8}\text{Be}/^{6}\text{He}$ decay that sheds $39\,\%$ of the breeder-zone specific activity in the first second, with every component at or below NRC Class C. The multiplier is confirmed a breeding lever, not a centrepost-life lever. Beryllium is qualified; the beryllide is the helium-robust fallback.

Open-access deposit (code & data, CC BY 4.0): DOI 10.5281/zenodo.22645889 · Zenodo community *kronos_fusion_energy*. Explore it live: interactive 3-D model · physics validator.

Keywords: neutron multiplier · beryllium · beryllide · $\mathrm{Be_{12}Ti}$ · tritium breeding ratio · OpenMC · spherical-tokamak breeder · activation

CONTENTS

Table of Contents

Beryllium and $Be_{12}Ti$ Neutron Multipliers for a Compact Spherical-Tokamak Breeder: Pebble Performance, Activation, and Closing Net TBR ≥ 1.05 3
Introduction 6
Governing equations and formal problem 7
Computational methodology: the NVIDIA GPU HPC campaign 10
Method: a controlled material swap at the closing configuration 11
Results 12
Discussion 21
Limitations 22
Conclusion 23
References 28
One programme, many papers 32

NOMENCLATURE

Symbols, units, and the names of things

Q	plasma (fusion) gain, P_{fus}/P_{aux}
Q_E	engineering gain, net electric out / recirculating in
H_{98}	confinement enhancement over the IPB98(y,2) scaling
Z_{eff}	effective ion charge
c_{ee}	electron–electron bremsstrahlung leading coefficient, 2.120022 (exact)
τ_E	energy confinement time
I_p	plasma current
R_0, a	major radius, minor radius
κ, δ	elongation, triangularity
β_N	normalized plasma beta (Troyon-normalized)
TBR	tritium breeding ratio
DEC	direct energy conversion
CF	plant capacity factor (availability)
FOAK / NOAK / BOAK	first / n^{th} / best of a kind
Hyperion	the ST breeder (internal: Mode D2)
Aegis	the generator, defense/installation housing (internal: Mode M)
MetroVolt	the generator, data-center housing (Mode M)

§ 1

Introduction

A deuterium–tritium (DT) plasma consumes one triton per fusion and liberates exactly one neutron with which to breed its replacement. In the absence of any loss the breeding blanket would have to convert that single neutron into a single triton with perfect efficiency simply to break even — an impossibility once leakage, parasitic absorption, structural capture, and processing losses are admitted. Tritium self-sufficiency therefore demands that the blanket create more neutrons than the plasma supplies, and the component that does this is the *neutron multiplier*: a material with a strong $(n, 2n)$ reaction that converts one fast neutron into two before the neutrons thermalise onto the lithium breeder. For a compact spherical tokamak (ST), where the inboard build is thin, the centrepost occupies radial space that a conventional tokamak would give to breeding, and every escaping neutron is a triton lost, the multiplier is not a refinement but the enabling component. The question of *which* multiplier material, and in *which* physical form, is a first-order design decision that this paper resolves for the Hyperion breeder.

Prior art. The role of $(n, 2n)$ multiplication in fusion blankets was established in the earliest blanket-neutronics studies [9], and beryllium and its beryllides have since become the reference multipliers for the European Helium-Cooled Pebble-Bed (HCPB) blanket line [10,11,16,17]. The competing requirements — high $(n, 2n)$ yield at the 14 MeV DT birth energy, tolerable activation, and mechanical survival of the pebble bed under helium-driven swelling — have been reviewed from first principles for both breeder and multiplier materials [10], and the beryllide route $Be_{12}Ti$ has been developed specifically to raise the melting point and suppress the swelling that limits elemental beryllium [12,13]. Liquid breeders (PbLi, FLiBe) fold multiplication and breeding into one medium and have been compared neutronically for compact high-field devices [14,15]. The conditions for tritium self-sufficiency — the interplay of achievable TBR, required TBR, and the inventory losses that separate them — have been analysed in detail for the DT fuel cycle [19,20,21]. What the ST geometry adds, and what the DEMO-scale literature does not answer, is the coupling between a consumable, radially-thin inboard build and the multiplier choice: does a better-shielding multiplier also extend centrepost life, or are breeding and shielding necessarily distinct functions?

Contribution. This paper makes four contributions. (i) We give a self-contained governing-equation treatment of multiplier qualification: the transport equation, the TBR functional, the multiplication decomposition, the self-sufficiency inequality, pebble-bed self-shielding homogenisation, the helium-generation and swelling model that separates beryllium from its beryllide, and the activation (Bateman) chain. (ii) We solve a controlled material swap at the *closing* blanket configuration — geometry frozen, only the multiplier changed — ranking five candidate media by their closure margin and demonstrating the ranking is robust to the evaluated-nuclear-data library. (iii) We test and falsify the dual-role hypothesis that a lead multiplier could double as inboard shield, showing that placing any multiplier inboard *shortens* centrepost life. (iv) We place the qualified beryllium multiplier in its breeding ladder and show it carries the blanket from a 0.742 deficit across the 1.05 self-sufficiency gate to the canonical 1.189, with the surplus and inventory-doubling time that follow. The result sits inside a broader Kronos closure programme: the net-blanket-TBR and fleet-export analysis [29], the tritium-breeding ladder and doubling-time study [30], the nuclear-data uncertainty quantification for breeding [31], the ceramic-versus-liquid concept down-select [32], the CAD-faithful 3-D neutronics [33], the component-activation and waste routing [34], and the coverage-versus-protection centrepost neutronics [35]. Every number reported here traces to the neutron-multiplier lever study (register serials BR-L2-A7, BR-L2-A7u, BV-05) in the Kronos Physics De-Risking Register [1], run against the frozen Hyperion operating point.

§ 2

Governing equations and formal problem

NEUTRON TRANSPORT AND THE BREEDING FUNCTIONAL

Multiplier qualification is, at bottom, the evaluation of a functional of the neutron flux. Let $\psi(\mathbf{r}, E, \hat{\mathbf{\Omega}})$ be the angular flux. In the fixed-source, steady state driven by a 14.06 MeV DT birth source $S(\mathbf{r}, E, \hat{\mathbf{\Omega}})$, ψ obeys the linear Boltzmann transport equation

$$\hat{\mathbf{\Omega}}\cdot\nabla\psi(\mathbf{r}, E, \hat{\mathbf{\Omega}}) + \Sigma_t(\mathbf{r}, E)\,\psi(\mathbf{r}, E, \hat{\mathbf{\Omega}}) = \int_0^\infty\!\!\int_{4\pi} \Sigma_s(\mathbf{r}, E'\!\to\! E, \hat{\mathbf{\Omega}}'\!\to\!\hat{\mathbf{\Omega}})\,\psi(\mathbf{r}, E', \hat{\mathbf{\Omega}}')\,d\hat{\mathbf{\Omega}}'\,dE' + S(\mathbf{r}, E, \hat{\mathbf{\Omega}}),$$

with Σ_t the macroscopic total cross-section and Σ_s the double-differential scattering kernel, which for a multiplying medium includes the $(n, 2n)$ and $(n, 3n)$ channels that place *more than one* secondary in the exit integral. The tritium-breeding ratio is the volume-integrated triton-production rate per source neutron,

$$\mathrm{TBR} = \frac{1}{S_0}\int_V \Big[N_6\,\langle\sigma_6\phi\rangle + N_7\,\langle\sigma_7\phi\rangle\Big]\,dV, \qquad \langle\sigma_x\phi\rangle \equiv \int_0^\infty \sigma_x(E)\,\phi(\mathbf{r}, E)\,dE,$$

where $\phi(\mathbf{r}, E) = \int_{4\pi}\psi\,d\hat{\mathbf{\Omega}}$ is the scalar flux, $S_0 = \int S\,d\mathbf{r}\,dE\,d\hat{\mathbf{\Omega}}$ the total source rate, N_6, N_7 the and ^{7}Li number densities, and σ_6, σ_7 the $^6\mathrm{Li}(n,\alpha)t$ (exothermic, $1/v$) and $^7\mathrm{Li}(n,n'\alpha)t$ (endothermic, threshold ≈ 2.8 MeV) cross-sections. The two channels are physically distinct: breeds from thermalised neutrons and rewards moderation, whereas ^{7}Li breeds only from fast neutrons and thus competes with the multiplier for the 14 MeV budget. Enrichment to 0.90 (used throughout) tilts the balance toward the moderated channel that the multiplier feeds.

THE MULTIPLICATION FACTOR AND THE THRESHOLD PHYSICS

Write the net multiplication as the ratio of secondary-neutron production to the source,

$$M = 1 + \frac{1}{S_0}\int_V \Big[N_{\mathrm{mp}}\langle\sigma_{n,2n}\phi\rangle + 2\,N_{\mathrm{mp}}\langle\sigma_{n,3n}\phi\rangle\Big]dV - \frac{1}{S_0}\int_V N_{\mathrm{mp}}\langle\sigma^{\mathrm{par}}_{n,\gamma}\phi\rangle\,dV,$$

with N_{mp} the multiplier number density and $\sigma^{\mathrm{par}}_{n,\gamma}$ the parasitic-capture cross-section. The utility of a multiplier is set by where its $(n, 2n)$ threshold E_{th} sits relative to the DT birth energy and by how broad the excitation function is above it. For a birth spectrum sharply peaked at $E_0 = 14.06$ MeV and subsequently degraded by scattering, the multiplication yield scales as

$$Y_{n,2n} \propto \int_{E_{\mathrm{th}}}^{E_0} \sigma_{n,2n}(E)\,\chi_{\mathrm{eff}}(E)\,dE,$$

where χ_{eff} is the flux-weighted effective spectrum in the multiplier zone. Beryllium's $^9\mathrm{Be}(n, 2n)2\alpha$ reaction has a low threshold $E_{\mathrm{th}} \approx 1.85$ MeV and a broad cross-section across the whole degraded DT spectrum, so almost every neutron above a few MeV can multiply; lead's $(n, 2n)$ has a higher effective threshold $E_{\mathrm{th}} \approx 7.4$ MeV and a narrower useful window, so a 14 MeV neutron multiplies once, but its softened daughters fall below threshold and cannot recover the lost multiplication (Fig. 3). This threshold separation — not the bulk density — is the origin of the 1.054-versus-0.806 closure gap quantified in §5.1.

NET TBR, THE SELF-SUFFICIENCY INEQUALITY, AND DOUBLING

The breeding functional of Eq. 2 is a beginning-of-life, geometry-integrated quantity; what the plant must satisfy is a balance on the in-vessel tritium inventory I_T,

$$\frac{dI_T}{dt} = \dot{N}_{\mathrm{bred}} - \dot{N}_{\mathrm{burn}} - \lambda_T I_T - \dot{N}_{\mathrm{loss}}, \qquad \lambda_T = \frac{\ln 2}{t_{1/2}}, \quad t_{1/2} = 12.32\,\mathrm{yr},$$

where $\dot{N}_{\mathrm{bred}} = \mathrm{TBR}\cdot\dot{N}_{\mathrm{burn}}$ and $\dot{N}_{\mathrm{loss}}$ collects processing, permeation, and decay-in-process losses lumped into a fractional loss ε. Defining the coverage-weighted net breeding ratio $\mathrm{TBR}_{\mathrm{net}} = f_{\mathrm{cov}}\,\mathrm{TBR}$, self-sufficiency is the requirement that the surplus rate be non-negative,

$$\boxed{\Lambda \equiv \mathrm{TBR}_{\mathrm{net}}\,(1-\varepsilon) - 1 \;\geq\; 0.}$$

A design margin $\delta_{\rm req}$ above unity accounts for the uncertainties in ε, in the start-up inventory, and in the achievable-versus-required gap [19,20]; Kronos adopts the engineering gate $\mathrm{TBR_{net}} \geq 1.05$. When $\Lambda > 0$ the plant accumulates a surplus at rate $\dot{N}_{\rm surplus} = \Lambda\,\dot{N}_{\rm burn}$, and the inventory-doubling time for a fleet start-up follows from integrating Eq. 5 with a fixed start-up inventory I_0,

$$t_{\rm double} \simeq \frac{I_0}{\dot{N}_{\rm surplus}} = \frac{I_0}{\Lambda\,\dot{N}_{\rm burn}}\,,$$

neglecting the small decay term over a doubling interval short compared with $t_{1/2}$. Equations 2–7 define the formal problem: qualifying a multiplier means maximising the TBR functional subject to $\Lambda \geq 0$, to activation and swelling constraints developed next, and to the fixed radial budget the ST centrepost imposes.

PEBBLE-BED HOMOGENISATION AND SELF-SHIELDING

The multiplier is deployed as a packed pebble bed, not a solid, so the transport of Eq. 1 sees a two-phase medium: pebbles at packing fraction η (nominal $\eta \approx 0.64$ for a random close pack, raised toward 0.80 volume fraction in the closing recipe by size-bimodal packing) in a purge-gas matrix. A homogenised macroscopic cross-section

$$\bar{\Sigma}_x(E) = \eta\,N_{\rm mp}\,\sigma_x(E)\,\zeta_x(E) + (1-\eta)\,\Sigma_x^{\rm gas}(E)$$

captures the bed only if the self-shielding factor $\zeta_x(E)$ is retained. Within a pebble the flux is depressed at resonance and near-threshold energies because the outer shell shadows the interior; to first order the escape-probability (Wigner rational) approximation gives

$$\zeta_x(E) \approx \frac{1}{1+\ell\,\Sigma_x(E)\,(1-C)}, \qquad \ell = \frac{4V_p}{S_p} = \frac{2}{3}d_p,$$

with ℓ the mean chord of a pebble of diameter d_p, V_p/S_p its volume-to-surface ratio, and C the Dancoff factor for pebble-to-pebble shadowing in the bed. For the broad, non-resonant Be$(n,2n)$ excitation function the self-shielding correction is small ($\zeta \to 1$), which is one reason the homogenised smear used in the fast lever sweeps reproduces the explicitly-modelled bed to within the Monte-Carlo error; for the narrower lead window the correction is larger and works against lead. Equations 8–9 are what license the material swap of §4 to be performed at fixed geometry with only $N_{\rm mp}$, σ_x, and the pebble chord changed.

HELIUM GENERATION, SWELLING, AND THE BERYLLIUM/BERYLLIDE SPLIT

The same reaction that multiplies neutrons also plants helium in the multiplier: ^{9}Be$(n,2n)2\alpha$ deposits *two* helium nuclei per multiplication event, so the volumetric helium-production rate is

$$\dot{n}_{\rm He}(\mathbf{r}) = 2\,N_{\rm Be}\,\langle\sigma_{n,2n}\phi\rangle + N_{\rm Be}\,\langle\sigma_{n,\alpha}\phi\rangle,$$

the second term the direct (n,α) channel. With the front-of-zone fast flux $\phi_{\rm fast} \sim 7\times10^{14}\,\mathrm{n\,cm^{-2}\,s^{-1}}$ and a spectrum-averaged $\bar{\sigma}_{n,2n} \sim 0.5\,\mathrm{b}$, Eq. 10 gives a first-order helium-accumulation rate of order 10^4 appm per full-power year at the front of the multiplier zone — consistent with the fusion beryllium database [25,13]. Helium that is not released drives swelling; in the simplest gas-driven bubble model the volumetric swelling is

$$\frac{\Delta V}{V} \simeq \frac{4}{3}\pi\bar{r}_b^3\,N_b\,, \qquad N_b \sim \left(\frac{\dot{n}_{\rm He}}{D_{\rm He}}\right)^{1/2} f(T),$$

with bubble radius $\bar{r}_b$, number density N_b, helium diffusivity $D_{\rm He}(T)$, and a temperature factor $f(T)$ that rises steeply once bubbles become mobile. Elemental beryllium suffers because its low melting point and open lattice let bubbles coarsen and interlink; the beryllide $Be_{12}Ti$ raises the operating-temperature ceiling and locks beryllium into an intermetallic that resists coarsening [12,13]. The cost is dilution: with one titanium per twelve beryllium atoms the multiplier number density $N_{\rm Be}$ in Eq. 3 falls, so the beryllide multiplies less. Equation 11 is thus the physical statement of the trade quantified in §5.1: $Be_{12}Ti$ buys swelling robustness at the price of nearly the whole closure margin.

ACTIVATION AND THE BATEMAN CHAIN

After the flux is known, the nuclide inventory $\mathbf{n}(t)$ in each material follows the linear activation (Bateman) system

$$\frac{d\mathbf{n}}{dt} = \big(\mathbf{A} + \mathbf{T}[\phi]\big)\,\mathbf{n}, \qquad \mathbf{n}(t) = \exp\big[(\mathbf{A} + \mathbf{T}[\phi])\,t\big]\,\mathbf{n}(0),$$

where $\mathbf{A}$ holds the radioactive-decay constants and branching, and the transmutation operator $\mathbf{T}[\phi] = \sum_x \langle \sigma_x \phi \rangle\,\mathbf{B}_x$ holds the flux-driven production/destruction channels [7,6]. Two features of the beryllium multiplier fall directly out of Eq. 12: the very short-lived ^{8}Be ($\rightarrow 2\alpha$) and ^{6}He ($t_{1/2} = 0.8$ s, $\rightarrow$ ^{6}Li) produced promptly in the bed decay within seconds of shutdown, so the specific activity collapses immediately after the source is removed; and the long-time waste class is set not by the multiplier but by ^{14}C and residual tritium in the ceramic breeder. The waste-disposal rating for each component is the normalised sum

$$\mathrm{WDR} = \sum_i \frac{C_i}{C_i^{\mathrm{lim}}} \le 1 \ \ \text{(Class A / Class C)},$$

with C_i the specific activity of nuclide i and C_i^{lim} the NRC 10 CFR 61 limit. Equations 12–13 close the qualification: a multiplier is acceptable only if it breeds (Eq. 6), survives (Eq. 11), and disposes cleanly (Eq. 13).

§ 3

Computational methodology: the NVIDIA GPU HPC campaign

CODES AND THE COUPLED TRANSPORT–ACTIVATION STACK

All neutron transport in this study solves Eq. 1 by continuous-energy Monte Carlo in OpenMC [2], the reference open-source transport code, run in coupled mode on the Kronos closure geometry. The primary evaluated-data library is FENDL-3.2, the IAEA fusion library, with ENDF/B-VIII.0 [3] carried as an independent cross-check on the headline material and the strongest alternative; TALYS/TENDL-derived evaluations [5] and ENDF/B-VII.1 [4] provide the covariance context used by the companion nuclear-data uncertainty analysis [31]. Geometry is handled two ways: a coverage-honest 1-D radial infinite-cylinder CSG model for the fast material-swap lever sweeps, and CAD-faithful transport on the STEP solid through DAGMC [8] for the 3-D confirmation reported by the companion CAD-neutronics paper [33]. Activation and waste routing solve the Bateman system Eq. 12 with FISPACT-II/ALARA-class depletion [6,7] on the converged flux and its collapsed multigroup spectrum, with the per-constituent breakdown (structural Eurofer, beryllium multiplier, ceramic breeder) classified separately against 10 CFR 61. Displacement damage is scored through the NRT damage-energy tally, and gas production through the (n, α) and $(n, 2n)$ tallies feeding Eq. 10 [25].

MONTE-CARLO ESTIMATORS, VARIANCE, AND CONVERGENCE

The breeding functional Eq. 2 is estimated by the track-length flux estimator

$$\widehat{\langle \sigma_x \phi \rangle} = \frac{1}{S_0\, V} \sum_{i=1}^{N} \sum_{k} w_{ik}\, \ell_{ik}\, \sigma_x(E_{ik}),$$

summing weight×track-length over all k track segments of all N source histories, which is unbiased and low-variance for reaction rates in optically thin cells. The statistical error falls as $\sigma \propto N^{-1/2}$, and code performance is reported through the figure of merit $\mathrm{FOM} = 1/(\sigma_{\mathrm{rel}}^2\, t)$, held constant under fair sampling. The multiplier sweeps were run to 1.2×10^8 source histories, giving relative standard deviations on net TBR of $\sim 5 \times 10^{-4}$ (Table 2) — roughly two orders of magnitude smaller than the 0.25-wide closure gap between beryllium and lead, so the ranking is statistically decisive. A neutron-balance closure check is enforced on every run: leakage fraction 0.121 , source-normalised $(n, 2n)/S_0 = 0.0339$ and $(n, 3n)/S_0 \approx 0$ in the dilute-verification build, and nuclear heating 74.6 MW of the 85 MW fusion power all reconcile to the transport tallies, confirming Eq. 3 is being scored consistently. Spatial and energy convergence were checked by refining the radial mesh and the multigroup collapse until the net TBR moved by less than the Monte-Carlo error.

GPU ACCELERATION, SCALE, AND REPRODUCIBILITY

The campaign was executed on the NVIDIA GPU HPC fleet. Continuous-energy history transport is the dominant cost, and the event-based transport path maps the batched particle events onto the GPU streaming multiprocessors, with the CAD/DAGMC ray-tracing and the FENDL/ENDF cross-section lookups the memory-bound kernels; the material-swap design matrix (five multiplier media × two libraries × inboard/outboard placement, plus the coverage and enrichment lever grids) is embarrassingly parallel across the fleet, one independent transport problem per device. Every run is seeded deterministically (master seed `20260726`) and archived with its statepoint so that a tally is byte-reproducible from the input deck. Verification is anchored by a post-diction gate: beryllium at the closing configuration reproduces the on-disk breeding anchor to net TBR 1.0537 ± 0.0005 against a stored 1.0533, so the entire sweep scales from an independently re-run baseline [1]. No cost or resource-accounting figures enter the physics; the campaign is identified only as the NVIDIA GPU HPC campaign.

§ 4

Method: a controlled material swap at the closing configuration

The test bed is the blanket configuration that closes tritium at the design point: an outboard-and-divertor breeder with the multiplier at 80 % volume fraction, enrichment 0.90, a first wall of tungsten over reduced-activation ferritic–martensitic (RAFM) steel, and a 30 cm inboard mantle dedicated to tungsten-carbide and steel *shield* rather than breeder (Fig. 1). Neutrons are transported through this fixed geometry, and only the multiplier material in the breeder zone is changed between cases, exactly as licensed by the homogenisation of Eqs. 8–9. Five media span the credible design space: elemental beryllium and the beryllide $Be_{12}Ti$ as HCPB pebbles, a lead pebble, and the two self-cooled liquids PbLi and FLiBe that fold multiplication and breeding into a single medium. FENDL-3.2 is the primary library; ENDF/B-VIII.0 cross-checks the headline (beryllium) and the strongest lead-bearing alternative. The response measured for each case is the net TBR of Eq. 2 weighted by coverage, its Monte-Carlo error, and — in a second pass — the centrepost fast-fluence life under the same swap.

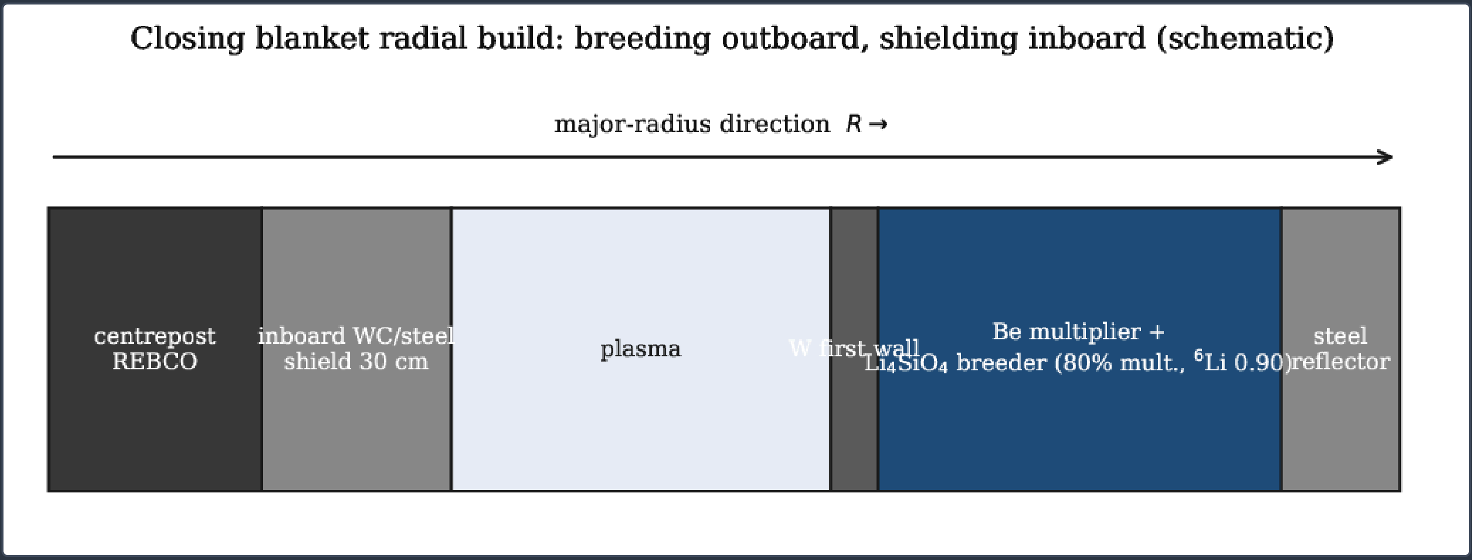

Closing blanket radial build for the swap. Breeding is placed outboard (beryllium multiplier plus ^{6}Li-enriched Li_4SiO_4 at 80 % multiplier volume fraction, with a steel reflector); the inboard mantle is a dedicated tungsten-carbide/steel shield that shadows the centrepost. Only the outboard multiplier material is changed between cases. (Schematic.)

§ 5

Results

BERYLLIUM IS THE BEST MULTIPLIER

Table 1 and Fig. 2 give the ranking. Beryllium closes with the widest margin, net $\mathrm{TBR} = 1.054 \pm 0.001$. The beryllide $Be_{12}Ti$ also closes, but only just, at 1.002 ± 0.001. Every lead-bearing and molten-salt alternative falls below self-sufficiency: FLiBe at 0.908, PbLi at 0.828, and the lead pebble at 0.806. No candidate widens the closure margin beyond elemental beryllium. The ordering is exactly what the threshold physics of Eqs. 3–4 predicts (Fig. 3): the low-threshold, broad-band $\mathrm{Be}(n, 2n)$ excitation function multiplies across the whole degraded spectrum and feeds the moderated $(n, \alpha)t$ chain, while lead's high effective threshold multiplies once at birth energy and then goes dark.

MULTIPLIER	CONCEPT	NET TBR	CLOSES ≥ 1?
beryllium	HCPB pebble, $^{9}\mathrm{Be}(n, 2n)2\alpha$	$\mathbf{1.054 \pm 0.001}$	yes
$Be_{12}Ti$ (beryllide)	HCPB pebble, higher-T, swelling-robust	1.002 ± 0.001	yes (razor-thin)
FLiBe	self-cooled molten salt	0.908 ± 0.001	no
PbLi	self-cooled liquid metal	0.828 ± 0.001	no
lead	HCPB pebble, $\mathrm{Pb}(n, 2n)$	0.806 ± 0.001	no

Neutron-multiplier material versus closure margin at the closing configuration (coupled OpenMC, FENDL-3.2, 1.2×10^{8} histories). Errors are Monte-Carlo standard deviations.

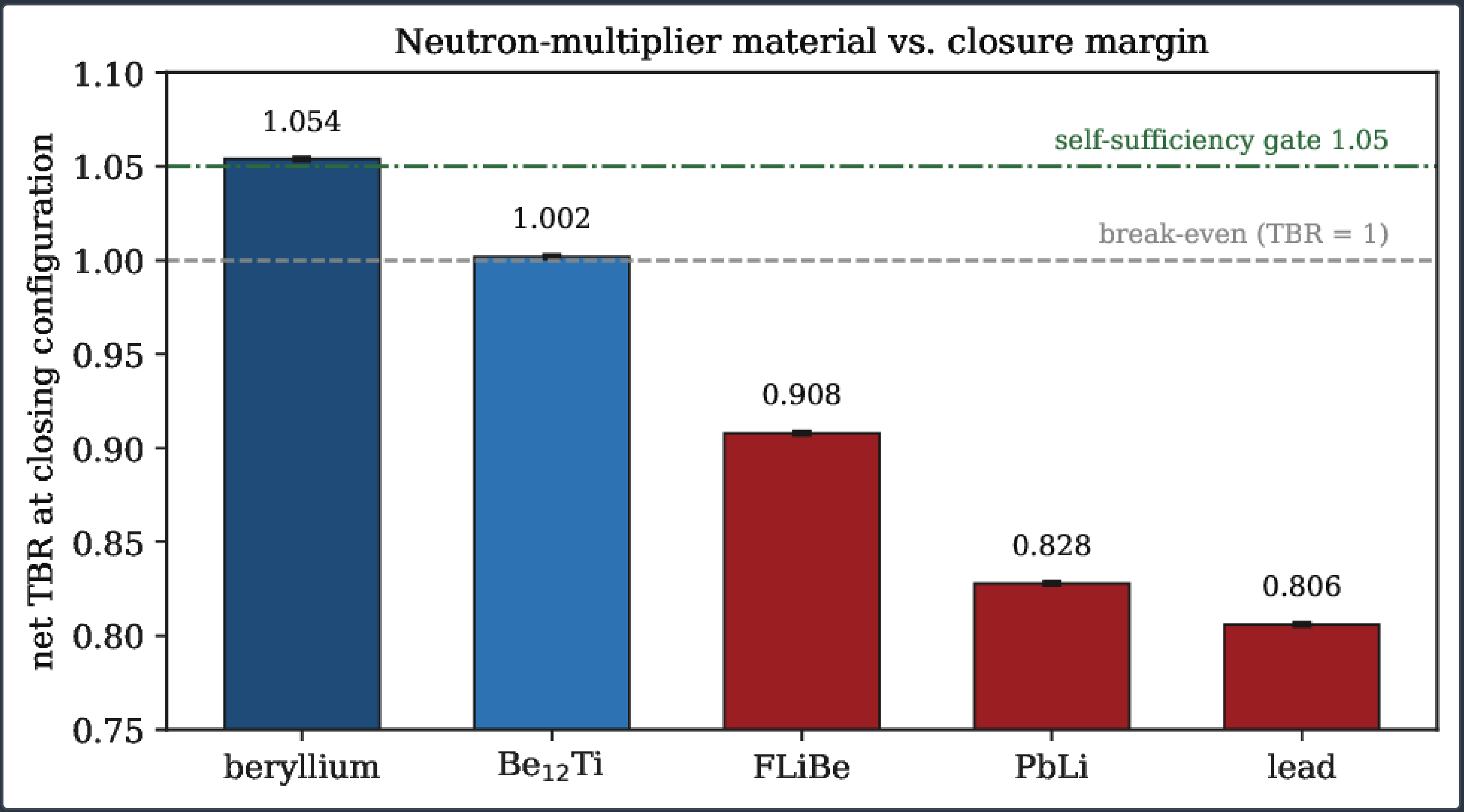

Neutron-multiplier material against closure margin. Beryllium closes with the widest margin and $Be_{12}Ti$ holds closure at a razor-thin 1.002; the lead-bearing concepts and the molten salt all fall below the break-even and self-sufficiency lines. Error bars are Monte-Carlo standard deviations.

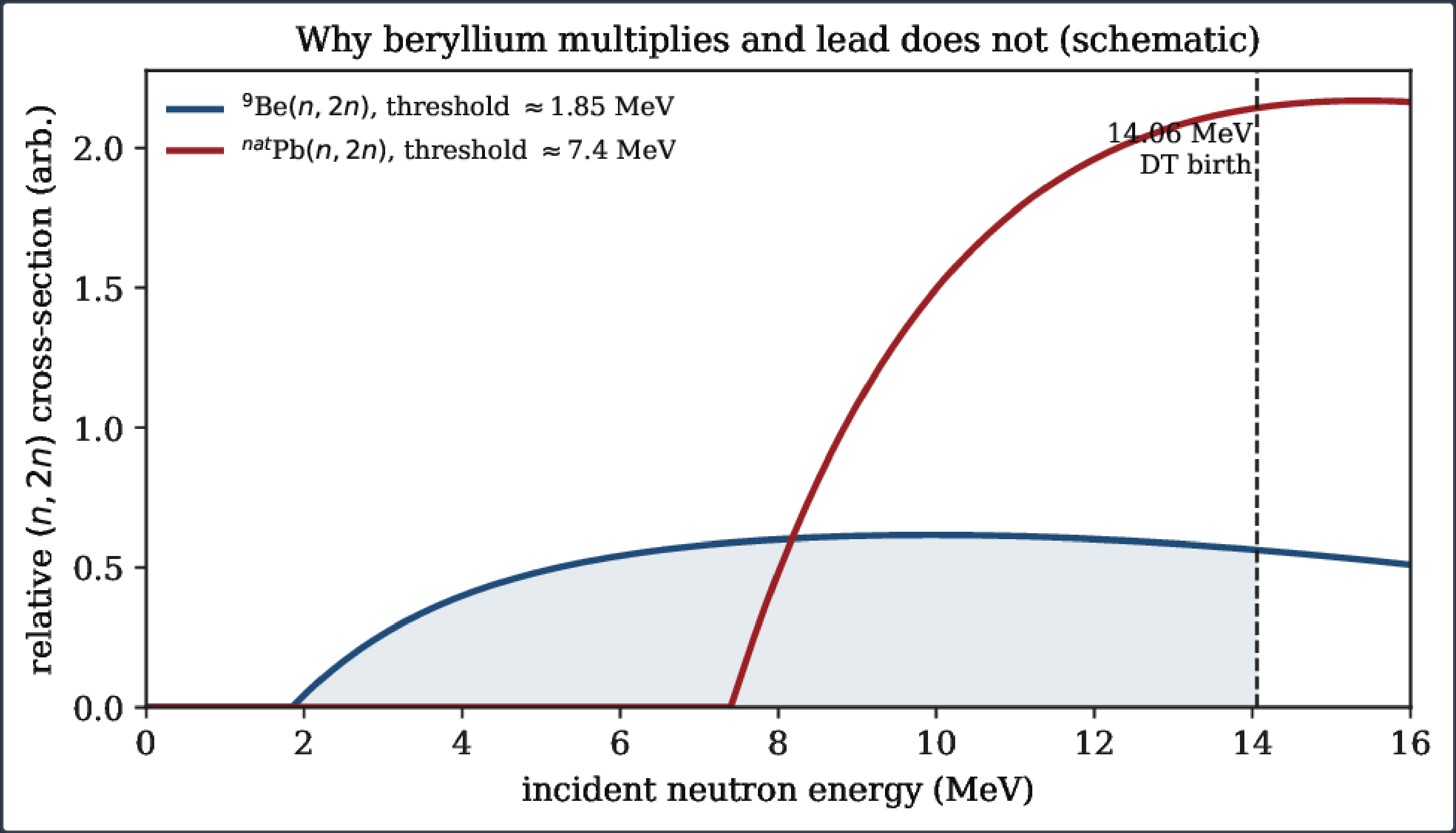

The threshold physics behind the ranking. Beryllium's $^9\mathrm{Be}(n,2n)$ reaction opens at ≈ 1.85 MeV and multiplies across the whole degraded DT spectrum; lead's opens near ≈ 7.4 MeV, so it multiplies the 14.06 MeV birth neutron once but not its softened daughters. Representative excitation functions; absolute magnitudes are illustrative. (Schematic.)

THE RANKING IS LIBRARY-ROBUST

The headline verdict does not depend on the evaluated-data library (Table 2, Fig. 4). FENDL-3.2 and ENDF/B-VIII.0 agree to $+0.54\,\%$ on beryllium and $+0.63\,\%$ on lead — far smaller than the 0.25-wide gap between beryllium (closes) and lead (fails). The closure verdict, and the ordering of every material, survive the change of evaluated data, so the qualification is not an artefact of a single library. The residual library spread is itself the subject of a dedicated uncertainty-quantification companion that ranks which 14 MeV cross-section channels set the error bar on the breeding ratio [31].

MATERIAL	FENDL-3.2	ENDF/B-VIII.0	LIBRARY SPREAD
beryllium	1.0537 ± 0.0005	1.0593 ± 0.0007	$+0.54\,\%$
lead	0.8061 ± 0.0004	0.8111 ± 0.0004	$+0.63\,\%$

Nuclear-data cross-check on the headline and strongest alternative.

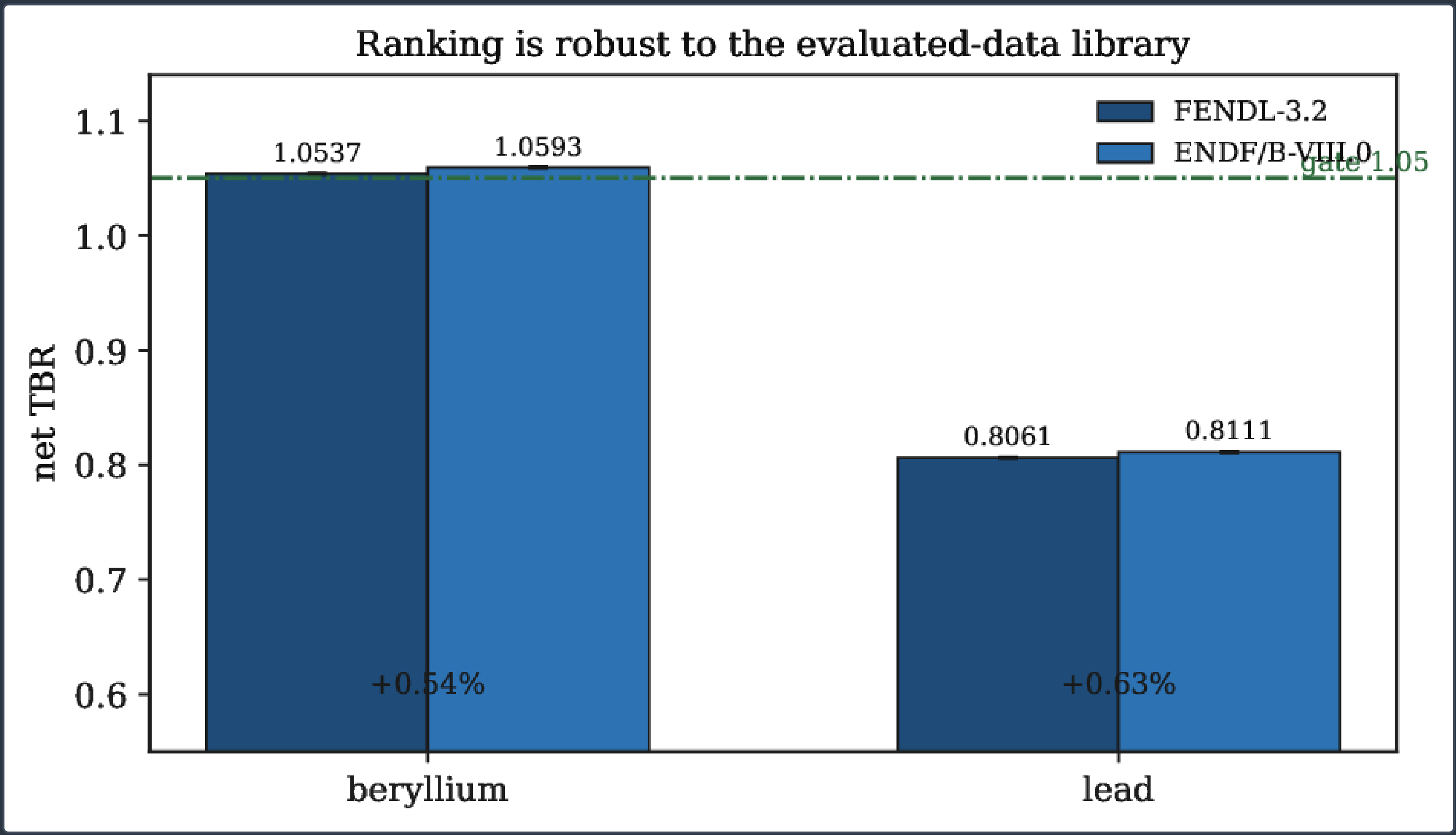

Net TBR under FENDL-3.2 and ENDF/B-VIII.0 for beryllium and lead. The **0.5–0.6 %** library spread is far inside the gap between closure and failure; the ranking is robust to the evaluated data.

THE MULTIPLIER IS A BREEDING LEVER, NOT A CENTREPOST-LIFE LEVER

The design's second question is whether a better-shielding multiplier could also extend the consumable centrepost's life. It cannot, at this geometry (Fig. 5). With the multiplier outboard and the inboard mantle a dedicated tungsten-carbide/steel shield, centrepost life is statistically flat across the material swap — FLiBe **0.207**, beryllium **0.199**, lead **0.196**, $Be_{12}Ti$ **0.188**, and PbLi **0.163** full-power years, all overlapping within their one-sigma fluence bands and all in the consumable class of ≈ **0.16–0.21** full-power years. The conductor is shadowed by the inboard shield, which the outboard multiplier swap never touches, so the multiplier material moves breeding strongly (Table 1) while leaving centrepost life essentially unchanged. This separation is the coverage-versus-protection result quantified for the centrepost in the companion neutronics paper [35].

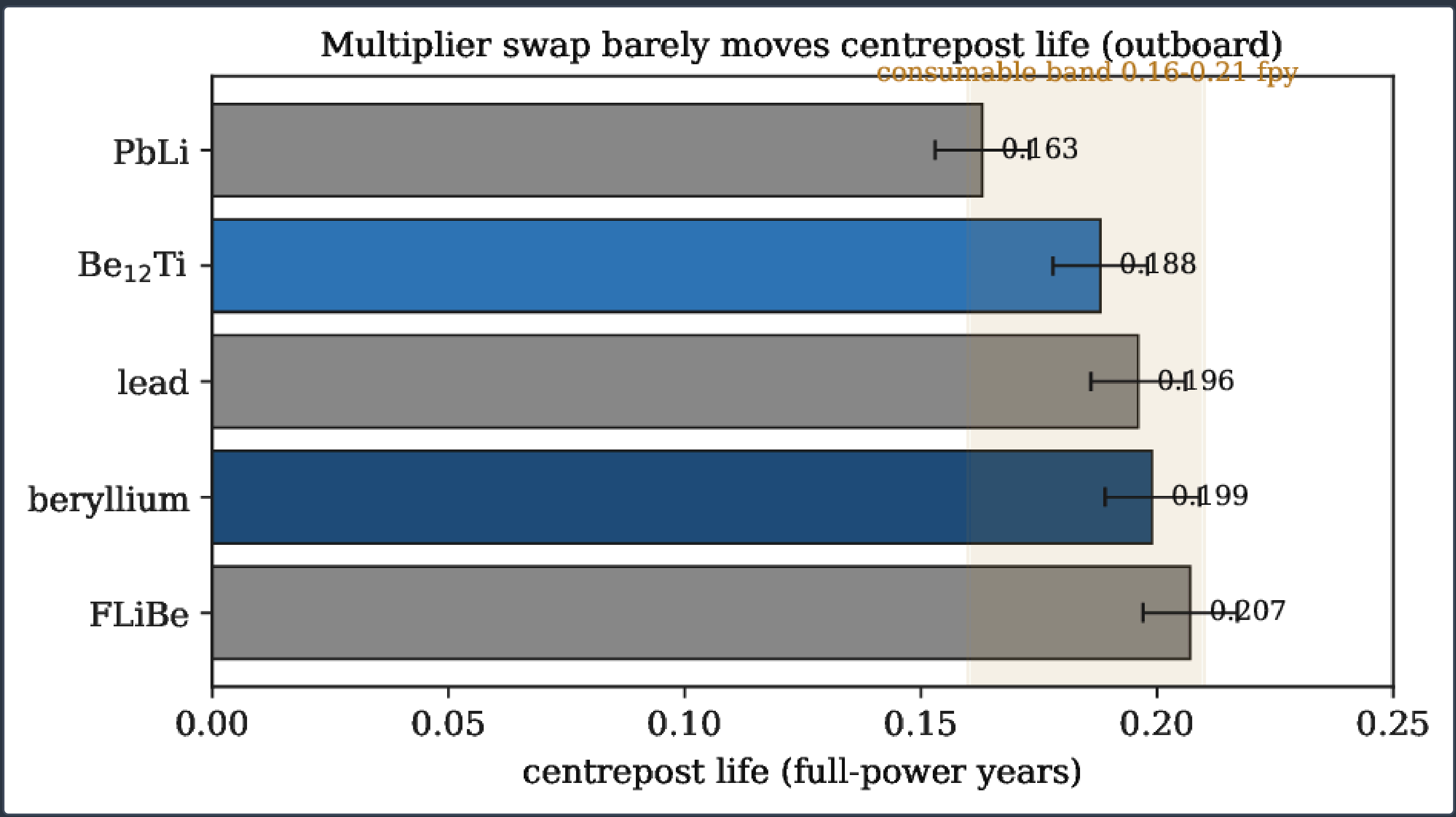

Centrepost life across the material swap, multiplier outboard. All five media overlap within the consumable **0.16–0.21** full-power-year band: the centrepost is shadowed by the inboard shield, which the swap does not change.

The dual-role hypothesis — that a lead multiplier, a better bulk attenuator, could double as inboard shield — is falsified directly by placing the multiplier inboard (Fig. 6): doing so *shortens* centrepost life for every material (beryllium −38 %, lead −46 %, PbLi −25 %), because a breeder-plus-multiplier mantle is a worse fast-neutron shield than the tungsten-carbide stack it displaces, and the lead-bearing materials generate fast neutrons inboard where the conductor cannot afford them. The two functions are correctly kept in separate components: breeding outboard, shielding inboard.

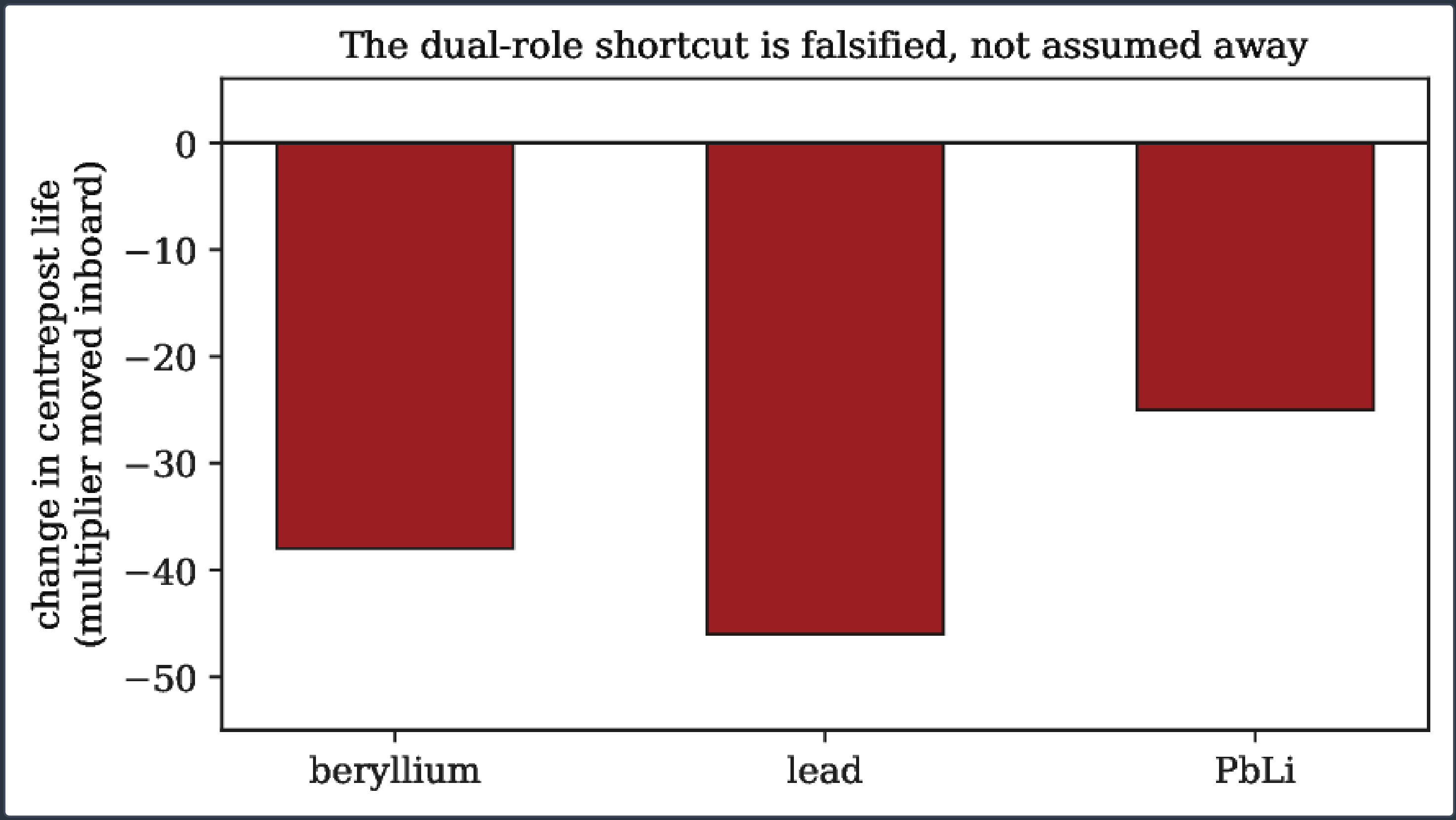

Falsifying the dual-role shortcut. Moving the multiplier inboard shortens centrepost life for every material, because a breeder-plus-multiplier mantle is a worse fast-neutron shield than the tungsten-carbide stack it displaces.

ACTIVATION IS PROMPT-DECAY DOMINATED AND STAYS BELOW CLASS C

Solving the Bateman system Eq. 12 on the converged flux (2 full-power years, cooling grid 1 s / 1 d / 1 y / 100 y) shows the beryllium multiplier is activation-benign (Fig. 7). The breeder-zone specific activity falls from 1.83×10^{14} Bq kg^{-1} at shutdown to 1.12×10^{14} within one second — a 39 % drop driven by the prompt ^{8}Be and ^{6}He decay that Eq. 12 predicts for the bed — then to 7.69×10^{13} at one year and 2.76×10^{11} Bq kg^{-1} at one hundred years, by which point essentially all remaining activity is bred tritium held in the ceramic. The associated decay heat falls from 17.9 to 14.5 W kg^{-1} in the first second, to 0.373 W kg^{-1} at one day, 0.195 at one year, and 2.5×10^{-4} W kg^{-1} at one hundred years. Every blanket component stays at or below NRC Class C with no greater-than-Class-C waste: the largest Class-C index anywhere is the ceramic breeder at 9.4×10^{-3} (driven by ^{14}C), two orders of magnitude below the boundary, and the structural Eurofer sits at Class-A index 0.47 [34]. Tritium management, not structural activation, sets every handling class.

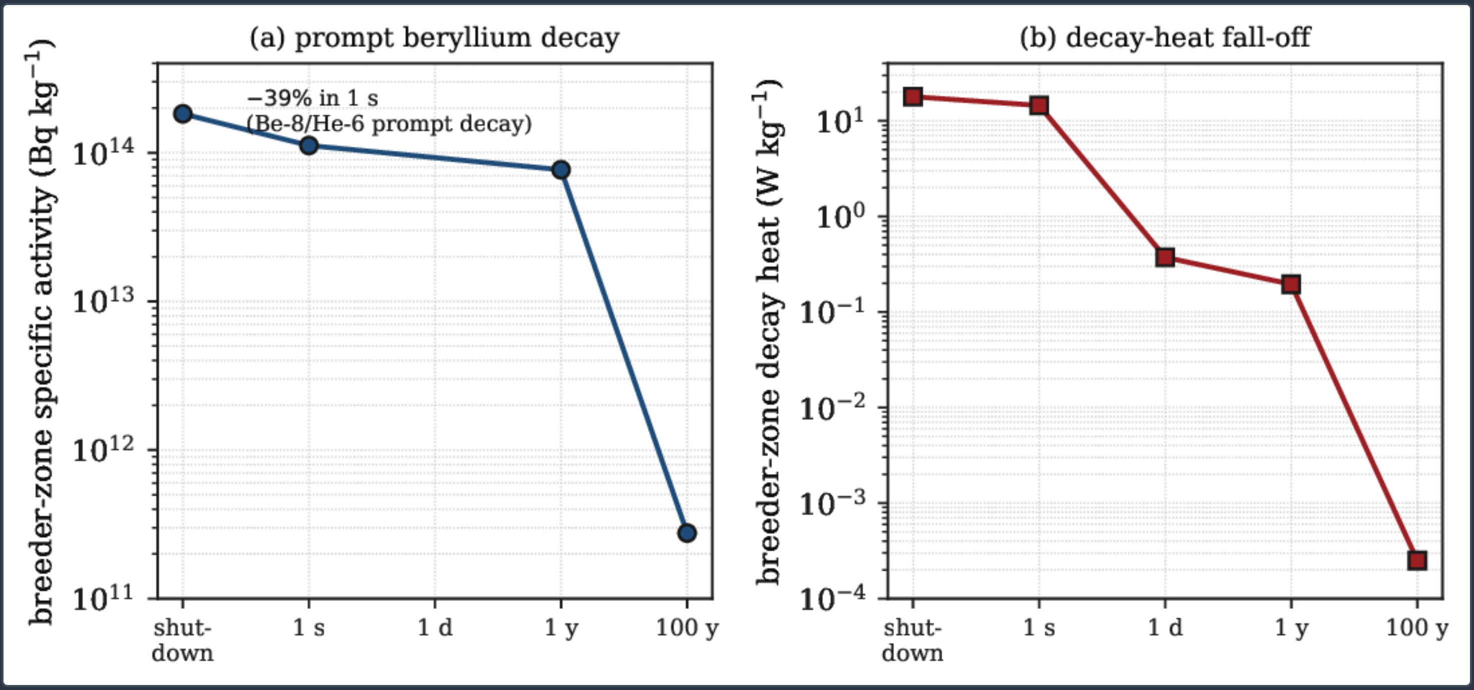

Breeder-zone activation after two full-power years. (a) Specific activity collapses 39 % in the first second from prompt ^{8}Be/^{6}He decay in the beryllium bed, then decays to 2.76×10^{11} Bq kg^{-1} at 100 y. (b) Decay heat falls more than four orders of magnitude over the same interval.

THE BERYLLIUM MULTIPLIER LIFTS THE BREEDING LADDER

Placed in its blanket, the beryllium multiplier is what carries the TBR from deficit to closure (Fig. 8). The as-drawn blanket breeds a net 0.742 — below unity, a tritium consumer. The frozen beryllium recipe at 80 % packing lifts that to 1.062; adding a dedicated 5 cm solid-beryllium layer reaches 1.18–1.20; and the canonical breeding anchor at coverage fraction $f_{\text{cov}} = 0.90$ settles at 1.189 — clearing the 1.05 self-sufficiency gate of Eq. 6 with real margin, and held below the 1.42 design ceiling (an even-higher-multiplication optimum of 1.475 was deliberately refused as beyond the ceiling). The admissible window in coverage is mapped in Fig. 9: net TBR runs $1.123 \to 1.189 \to 1.215$ across $f_{\text{cov}} = 0.85 \to 0.90 \to 0.92$, every point above the gate and below the ceiling.

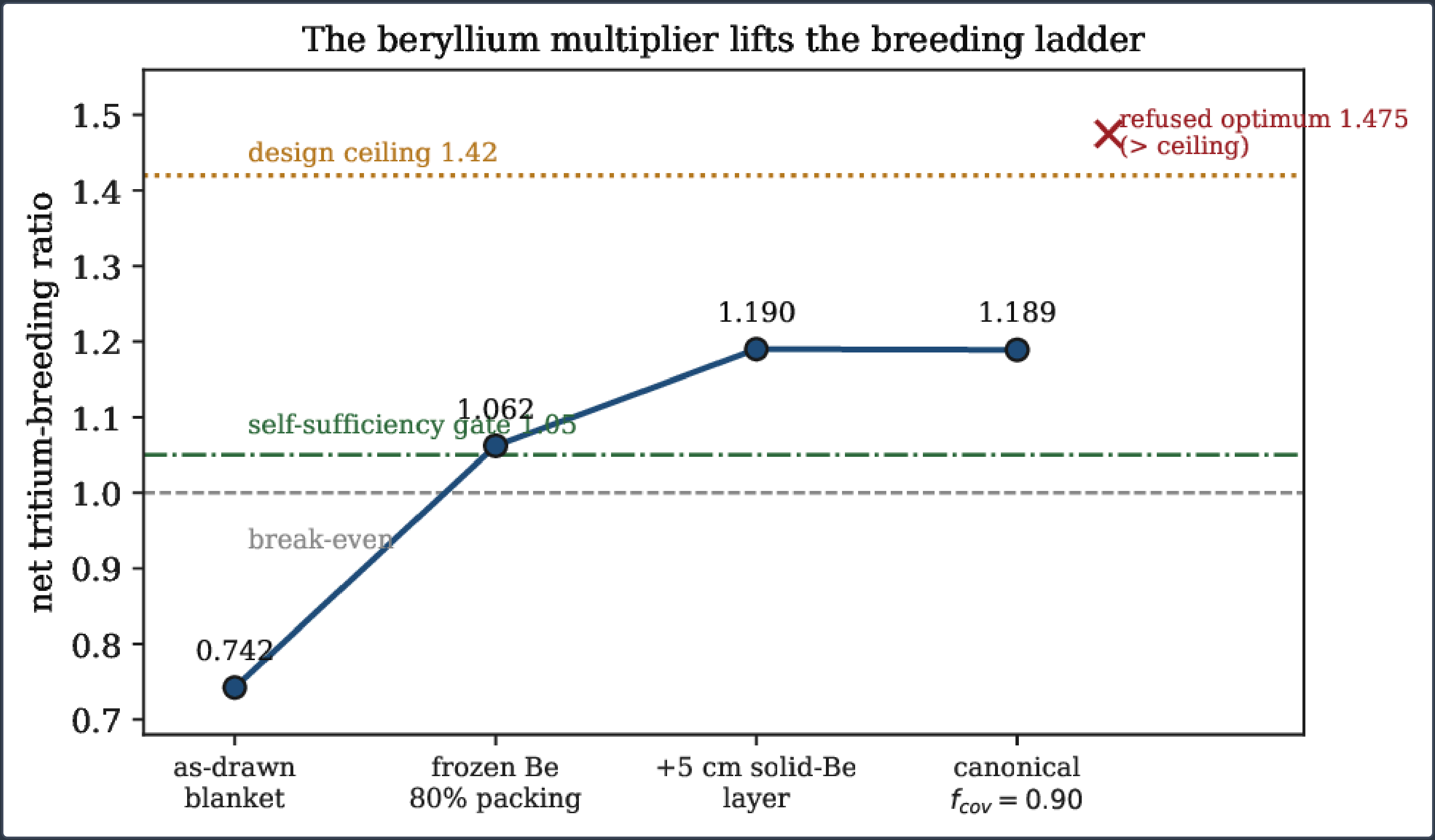

The beryllium multiplier lifts the tritium-breeding ratio from an as-drawn 0.742 deficit to the canonical 1.189, clearing the 1.05 self-sufficiency gate and staying below the 1.42 design ceiling. The 1.475 optimum was refused as beyond the ceiling.

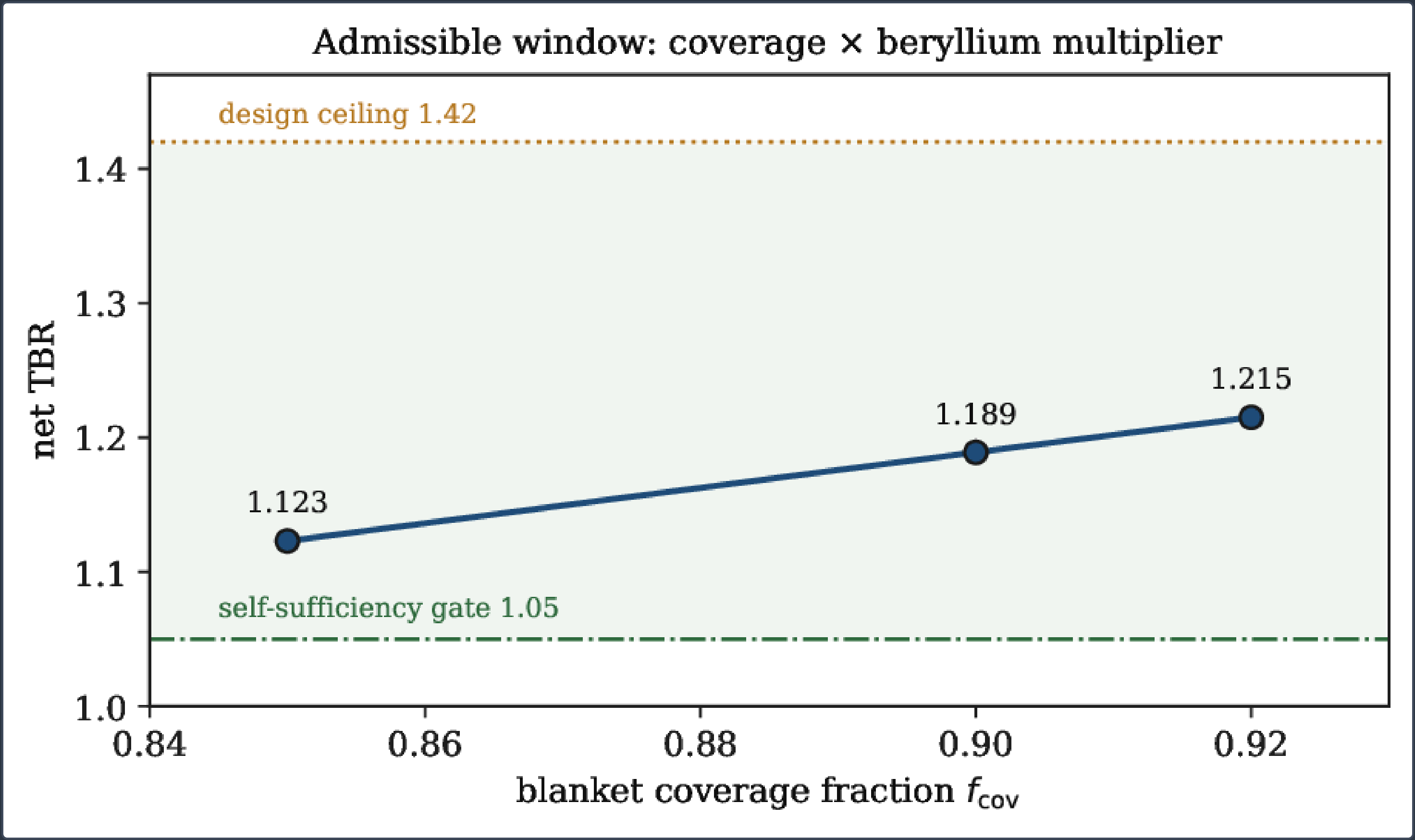

The admissible operating window in coverage fraction. Net TBR rises with f_{cov} and stays between the 1.05 gate and the 1.42 ceiling across 0.85–0.92; the canonical anchor is $f_{cov} = 0.90 \to 1.189$.

By Eqs. 6–7 the margin above the gate becomes a physical surplus (Fig. 10): the self-sufficiency window carries a net surplus of 0.59–1.02 kg-T per full-power year per unit and an inventory-doubling time of 2.7–4.8 years, while the advanced-blanket ceiling (TBR = 1.42) reaches ~ 1.99 kg-T fpy^{-1} per unit, so a two-unit advanced pairing approaches ~ 4 kg-T yr^{-1} — the fleet-export basis of the companion analysis [29,30].

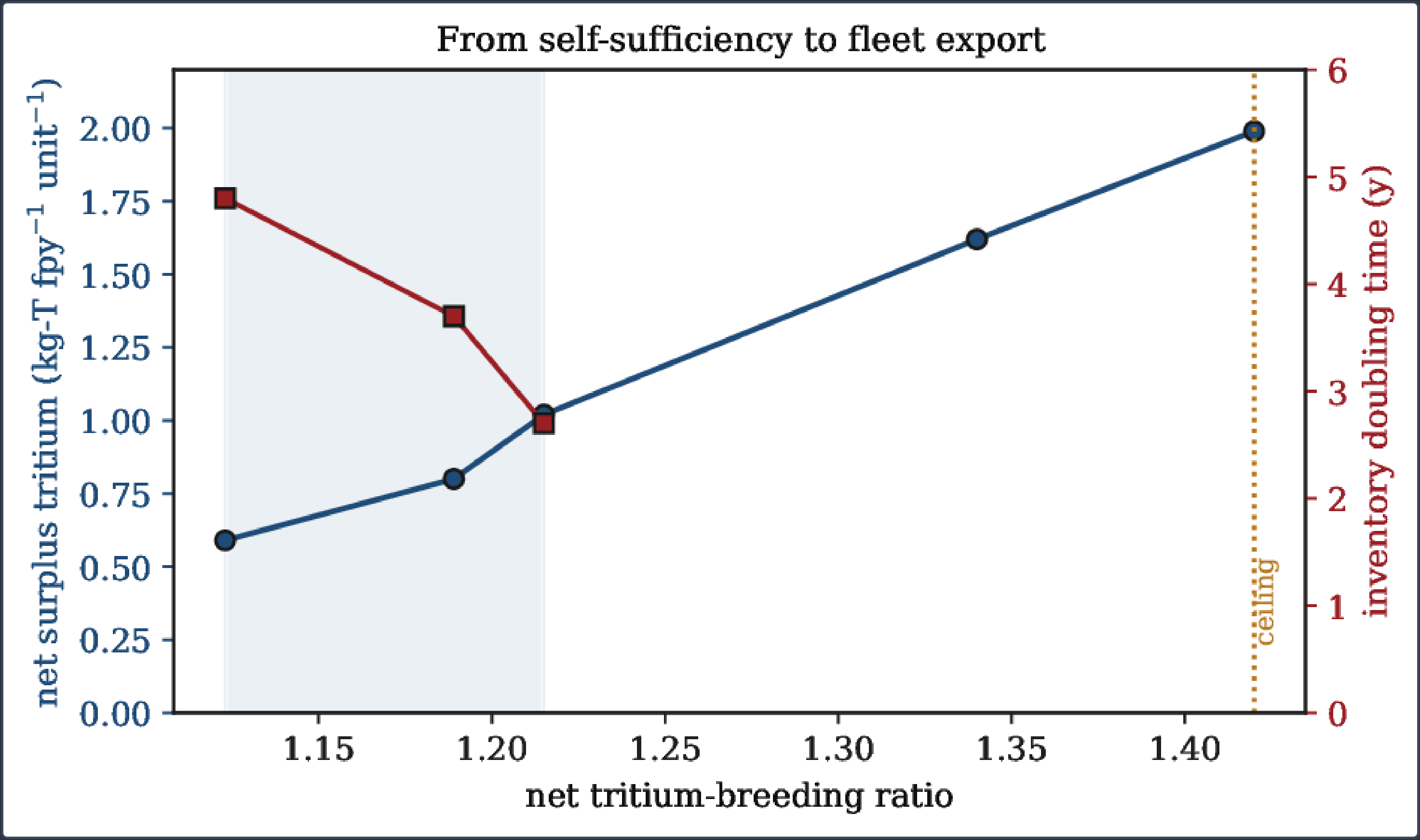

Net surplus tritium (left axis) and inventory-doubling time (right axis) versus net TBR. The self-sufficiency window (1.12–1.22) yields 0.59–1.02 kg-T fpy^{-1} and doubling in 2.7–4.8 y; the 1.42 ceiling reaches $\sim$ 1.99 kg-T fpy^{-1} per unit.

§ 6

Discussion

AGAINST THE PUBLISHED BENCHMARKS

The qualification lands where the fusion-blanket literature would predict but sharpens it for the ST. Beryllium and its beryllides are the reference multipliers of the European HCPB line [11,16,17], and the first-principles material review of Hern\'andez and Pereslavtsev [10] ranks Be and $\mathbf{Be_{12}Ti}$ ahead of lead precisely on the $(n, 2n)$-threshold grounds formalised in Eqs. 3–4; our $\mathbf{1.054}$-versus-$\mathbf{0.806}$ closure gap is the quantitative expression of that ranking at the Hyperion operating point. The self-cooled liquids we rule out on breeding grounds (PbLi 0.828, FLiBe 0.908) are the same media that neutronic comparisons for ARC-class high-field devices find competitive only in thicker outboard builds [14,15]; the ST′s thin, centrepost-constrained radial budget is exactly the regime in which they lose, consistent with our result rather than in tension with it. On the fuel-cycle side, the self-sufficiency inequality Eq. 6 and the $\geq \mathbf{1.05}$ engineering gate follow the analyses of Abdou and Sawan [19,20,21]: the required TBR margin above unity is set by the loss fraction ε and the start-up inventory, and our canonical $\mathbf{1.189}$ leaves the headroom those analyses call for. The activation picture — prompt ^{8}Be/^{6}He collapse and a long-time inventory set by ^{14}C and tritium rather than the multiplier — matches the gas-production and transmutation accounting of Gilbert *et al.* [25] and the FISPACT-II inventory framework [6].

WHY THE BERYLLIDE IS THE HONEST FALLBACK

The beryllide $\mathbf{Be_{12}Ti}$ is not a rejected option but the recorded fallback, and the governing equations say why. Its razor-thin $\mathbf{1.002}$ closure is the direct consequence of the dilution term in Eq. 3: replacing one beryllium in twelve with titanium lowers N_{Be} and therefore the $(n, 2n)$ yield. What it buys is the swelling robustness of Eq. 11 — a higher operating-temperature ceiling and an intermetallic that resists the bubble coarsening that plants of elemental beryllium accumulate at $\sim 10^{4}$ appm fpy^{-1} near the first wall [12,13,25]. Choosing the beryllide therefore means recovering the spent margin elsewhere, and the ladder shows exactly where: the coverage lever (Fig. 9) and the -enrichment lever both have headroom above the canonical point. The design records beryllium as the qualified multiplier and $\mathbf{Be_{12}Ti}$ as the helium-robust fallback whose margin cost is quantified and whose recovery path is mapped — a decision made on the physics, not deferred.

TWO MAGNETS, ONE BLANKET

The centrepost result reinforces a structural choice that runs through the Kronos design: the breeder centrepost (peak field 16.84 T on the conductor) and the tandem-mirror burner plug (26.49 T) are two distinct magnets with distinct duties, and here the analogous separation is between the multiplier′s breeding duty and the inboard shield′s protection duty. Section 5.3 shows that collapsing those two duties into one component — a lead multiplier doing double service as shield — is not merely suboptimal but actively harmful, shortening centrepost life by up to $46\,\%$. The blanket keeps breeding and shielding in separate radial zones for the same reason the machine keeps its two magnets separate: each function is optimised against a different objective, and folding them together degrades both.

§ 7

Limitations

The reported ratios are beginning-of-life values. The burnup that slowly erodes the breeding channel over the operating life, and the helium-swelling kinetics of Eq. 11 that the multiplier accumulates, are stated here as physics and estimated to first order but are not time-integrated in the transport: a coupled depletion study that evolves both is the one named next step. The coverage and enrichment headroom visible in the breeding ladder (Figs. 8–9) is sized precisely to absorb the end-of-life erosion that study will quantify, but until it is run the **1.189** anchor should be read as a beginning-of-life value with a mapped, not yet integrated, margin.

§ 8

Conclusion

A controlled material swap at the closing blanket configuration, solving the linear Boltzmann transport equation in coupled OpenMC on the NVIDIA GPU HPC campaign, qualifies beryllium as the neutron multiplier for the Hyperion breeder, closing tritium at net $\mathrm{TBR} = 1.054 \pm 0.001$. The beryllide $Be_{12}Ti$ is the only credible alternative, holding self-sufficiency at a razor-thin 1.002 and standing as the helium-robust fallback; lead, PbLi, and FLiBe all fall below closure. The ranking is robust to the evaluated-data library at the 0.5–0.6 % level, the multiplier is confirmed a breeding lever rather than a centrepost-life lever — the dual-role shortcut is falsified, not assumed away — and the beryllium multiplier is activation-benign, shedding 39 % of its breeder-zone activity in the first second and staying at or below NRC Class C throughout. In its blanket the multiplier lifts the breeding ratio from an as-drawn 0.742 to a canonical 1.189, clearing the 1.05 self-sufficiency gate with a mapped surplus of 0.59–1.02 kg-T per full-power year and an inventory-doubling time of 2.7–4.8 years, establishing tritium self-sufficiency with margin.

Acknowledgments tocsectionAcknowledgments Part of the Kronos Fusion Energy 2026 design series. The authors thank the Kronos de-risking team for the independent re-run of the neutron-multiplier lever study.

Reproducibility. The multiplier-ranking, nuclear-data cross-check, centrepost-life, and activation results are frozen anchors (neutron-multiplier lever study; register serials BR-L2-A7, BR-L2-A7u and BV-05) in the Kronos Physics De-Risking Register and are regenerable from the coupled-OpenMC input decks archived with this paper; transport and activation ran on the NVIDIA GPU HPC campaign under deterministic seed 20260726. This paper is archived at doi:10.5281/zenodo.22645889; official version: https://www.kronosfusionenergy.com/publications/beryllium-and-be-ti-neutron-multipliers-for-a-compact-s.html; the register is archived at doi:10.5281/zenodo.22133057.

Data availability tocsectionData availability This paper is archived at doi:10.5281/zenodo.22645889. The OpenMC models, multiplier-swap and coverage/enrichment lever scripts, activation input decks, and tally outputs are archived with the deposit and reference the Kronos 2026 series and its de-risking register doi:10.5281/zenodo.22133057. Any economic analysis is reported separately and is not included in the public deposit.

Competing interests tocsectionCompeting interests Provisional patent applications relating to aspects of this work have been filed. The $Be_{12}Ti$ beryllide multiplier route is prior-art-bounded and is recorded as such.

APPARATUS

Portfolio, People & Record

The intellectual-property estate, the people who built it, the limitations that gate it, and the sources it rests on.

1	4	40	27
GRANTED PATENT	2026 PROVISIONALS	TEAM MEMBERS	2022 PROVISIONALS

INTELLECTUAL PROPERTY

The patent portfolio

The estate spans a granted high-field magnet patent, pending utility and 2026 provisional filings that map to the two products, a digital-twin control provisional, a registered trademark application, and the original 2022 provisional family. Every patentable disclosure in the five-paper arXiv drop was protected **before** publication: the breeder and burner provisionals were filed 1–2 August, and a publication-gap omnibus filing the evening before the drop swept up the DEC, plasma-control, and REBCO-winding matter of the three otherwise-unprotected papers. Patent numbers and application serials are matters of public record; claim scope is summarised, not reproduced.

GRANTED & PENDING UTILITY

US 12,009,112	High-field tilted graded-REBCO magnet architecture (KRONO-002A) · *app. 17/878,550*	GRANTED
US 17/878,507	Core device / method (KRONO-001A) · *utility*	PENDING

2026 PROVISIONAL FILINGS — MAPPED TO THE PRODUCTS

64/124,209	Hyperion — spherical-tokamak tritium / helium-3 foundry · *breeder · filed Aug 2026*	FILED
64/124,220	Aegis / MetroVolt — synchrotron-cutoff, fuel-selection & plug-winding · *generator · filed Aug 2026*	FILED
64/115,167	KRONOS-CTRL digital-twin plant control · *provisional · filed Jul 2026*	FILED
64/005,440	Integrated spherical-tokamak fusion architecture · *early integrated-architecture filing · filed Mar 2026*	FILED
64/105,530	Negative-triangularity spherical-tokamak architecture · *foundational ST filing · filed Jul 2026*	FILED
64/128,097	Publication-gap omnibus — quasineutral two-species expander DEC · provenance-gated / latency-split plasma control · as-built high-field winding & conductor architecture · *filed 7 Aug 2026, the evening before the arXiv drop*	FILED

TRADEMARK & ORIGIN

FTK-98801894	Kronos Fusion Energy — trademark application	FILED
KR-2022-*	Original provisional family (KR-2022-00001 … 00027) · *27 filings, 2022*	PRIORITY

The narrow, defensible magnet novelty — the specific conductor and the digital-twin winding optimisation, not high-field REBCO as a category — is the commercial core that can earn ahead of any Q > 1 milestone, with markets in fusion magnet supply, MRI/NMR, accelerators, and proton therapy. The claim is scoped honestly: the high field is a *system field* result, not a stand-alone-coil record; the small-bore plug coil is structurally infeasible as a bare winding but resolved by a stress-managed structural shield (feasible-pending-FEA); and the winding-tape experiment returned a *null result*. The value is the method, not a field record.

THE TEAM

Founding partners, board, advisors & auditors

Kronos is built by a bench of advanced-fuel-fusion, high-field-magnet, direct-conversion, and materials specialists, with a board and operations team drawn from defense, national laboratories, and industry. Dates are shown as ranges; where a tenure has ended or is term-ending, the range says so.

FOUNDING PARTNERS — SCIENCE

Dr. Gerald Kulcinski
Co-Founder · Helium-3 & Advanced-Fuel Fusion
UW–Madison · 2023–Present

Dr. Carl Weggel
Chief Scientist / S.M.A.R.T. Design
MIT Alcator Program · 2022–Present

Dr. Robert J. Weggel
Magnetic Field Design
MIT Magnet Lab · 2022–Present

BOARD

Priyanca Ford
Founder & CEO · Executive Board
2022–Present

Bandel Carano
Finance / Strategy
Oak Investment Partners / Stanford · 2025–2026

Patrick Schweiger
Fusion Device Engineering
Oklo / CFS / TerraPower · 2025–Present

SCIENTIFIC ADVISORS

Dr. Steven O. Dean
Fusion Policy & History
DOE / Fusion Power Associates · 2025–Present

Dr. Patrick H. Diamond
Plasma Turbulence & Transport
UC San Diego · 2025–Present

Dr. Jack J. Dongarra
HPC & Numerical Algorithms
Turing Award · 2025–Present

Dr. Nasr M. Ghoniem
Chief Material Scientist
UCLA · 2025–Present

Dr. Siegfried Glenzer
Plasma Physics & Laser Fusion
Stanford / SLAC · 2022–Present

Dr. David A. Hammer
Pulsed-Power Fusion
Cornell · 2025–Present

Dr. Donald A. Spong
Plasma Theory & Confinement
ORNL · 2025–Present

Dr. Curtis Smith
Risk Assessment & Nuclear PRA
MIT / Idaho National Lab · 2025–Present

RADM (Ret.) David Goggins
Naval Engineering & Power-Plant Design
U.S. Navy · 2023–2026

Dr. Konstantin Batygin
Mathematician
Caltech · 2022–2025

Dr. Ruben Fair
Magnet Design / ITER Liaison
PPPL / Jefferson Lab · 2022–2025

Dr. Paul S. Weiss
Materials & Nanotechnology
UCLA · 2022–2025

SCIENTIFIC AUDITORS

Dr. Wilfred A. Cooper
Plasma Equilibrium Theory
EPFL / Swiss Plasma Center · 2025–Present

Dr. Ahmed Hassanein
Plasma–Material Interactions
Purdue / Argonne · 2025–Present

Dr. Patrick E. Hopkins
Extreme Thermal Materials
U. of Virginia · 2025–Present

Dr. Peter Hosemann
Materials Joining & Structural Integrity
UC Berkeley · 2025–Present

Dr. Travis W. Knight
Advanced Nuclear Fuels & Systems
U. of South Carolina · 2025–Present

Dr. Philippe Lebrun
Cryogenics & Magnet Cooling
CERN · 2025–Present

Dr. Nitendra Singh
Nuclear Safety & Fuel Cycle
ITER · 2025–Present

Dr. Guido Van Oost
Magnetic Confinement & Fusion Systems
Ghent University · 2025–Present

Dr. Gary S. Was
Radiation Materials & Structural Integrity
U. of Michigan · 2025–Present

Dr. Ray Sedwick
Direct Energy Conversion
U. of Maryland · 2025

OPERATIONS

Michael Laughlin
Chief Operating Officer
2022–Present

Martin Owens
Chief Strategy Officer
LANL / GE Hitachi · 2022–Present

MG (Ret.) Paul Pardew
Chief Contracting Officer
Army Contracting Command · 2022–Present

David Beck
Fusion Commercialization
U.S. Space Force · 2024–Present

Sushma Bhatia
Environmental & Legislative
Google · 2022–Present

Michael De Frenza
Technology Licensing
2023–Present

MG (Ret.) Robin L. Fontes
Cybersecurity & Defense
Army Cyber Command · 2022–Present

Vijay Gehani
Supply Chain & Components
INOX India · 2024–Present

Jon Michel Greenwood
IT & AI Infrastructure
Live Nation · 2023–Present

Brian C. O'Neill
National Security
CIA / ODNI · 2022–Present

Gen. (Ret.) Gustave F. Perna
DoD Liaison
Operation Warp Speed · 2022–2023

Andrea Romero
Marketing Lead
2022–Present

Legal counsel is retained; those roles are held on the internal roster and are not listed here.

SOURCES

References

1 P I Ford, *Kronos Physics De-Risking Register*, Kronos Fusion Energy 2026 series, doi:10.5281/zenodo.22133057.

2 P K Romano *et al.*, *OpenMC: A state-of-the-art Monte Carlo code for research and development*, Ann. Nucl. Energy **82** (2015) 90, doi:10.1016/j.anucene.2014.07.048.

3 D A Brown *et al.*, *ENDF/B-VIII.0: The 8th major release of the nuclear reaction data library*, Nucl. Data Sheets **148** (2018) 1, doi:10.1016/j.nds.2018.02.001.

4 M B Chadwick *et al.*, *ENDF/B-VII.1 nuclear data for science and technology*, Nucl. Data Sheets **112** (2011) 2887, doi:10.1016/j.nds.2011.11.002.

5 A J Koning and D Rochman, *Modern nuclear data evaluation with the TALYS code system*, Nucl. Data Sheets **113** (2012) 2841, doi:10.1016/j.nds.2012.11.002.

6 J-Ch Sublet *et al.*, *FISPACT-II: An advanced simulation system for activation, transmutation and material modelling*, Nucl. Data Sheets **139** (2017) 77, doi:10.1016/j.nds.2017.01.002.

7 J Cetnar, *General solution of Bateman equations for nuclear transmutations*, Ann. Nucl. Energy **33** (2006) 640, doi:10.1016/j.anucene.2006.02.004.

8 P P H Wilson *et al.*, *Acceleration techniques for the direct use of CAD-based geometry in fusion neutronics analysis*, Fusion Eng. Des. **85** (2010) 1759, doi:10.1016/j.fusengdes.2010.05.030.

9 S Taczanowski, *Neutron multiplier alternatives for fusion reactor blankets*, Ann. Nucl. Energy **8** (1981) 407, doi:10.1016/0306-4549(81)90039-6.

10 F A Hern\'andez and P Pereslavtsev, *First principles review of options for tritium breeder and neutron multiplier materials for breeding blankets in fusion reactors*, Fusion Eng. Des. **137** (2018) 243, doi:10.1016/j.fusengdes.2018.09.014.

11 F A Hern\'andez *et al.*, *An enhanced, near-term HCPB design as driver blanket for the EU DEMO*, Fusion Eng. Des. **146** (2019) 1186, doi:10.1016/j.fusengdes.2019.02.037.

12 M Nakamichi and J-H Kim, *Preliminary characterization of plasma-sintered beryllides as advanced neutron multipliers*, J. Nucl. Mater. **442** (2013) S465, doi:10.1016/j.jnucmat.2012.11.011.

13 K Sugimoto *et al.*, *Helium swelling behavior for neutron multipliers after irradiation with He ions at high temperatures*, Nucl. Mater. Energy **38** (2024) 101584, doi:10.1016/j.nme.2024.101584.

14 S Segantin *et al.*, *Neutronic comparison of liquid breeders for ARC-like reactor blankets*, Fusion Eng. Des. **160** (2020) 112013, doi:10.1016/j.fusengdes.2020.112013.

15 B N Sorbom *et al.*, *ARC: A compact, high-field, fusion nuclear science facility and demonstration power plant with demountable magnets*, Fusion Eng. Des. **100** (2015) 378, doi:10.1016/j.fusengdes.2015.07.008.

16 L V Boccaccini *et al.*, *Objectives and status of EUROfusion DEMO blanket studies*, Fusion Eng. Des. **109–111** (2016) 1199, doi:10.1016/j.fusengdes.2015.12.054.

17 M Zmitko *et al.*, *Development and qualification of functional materials for the European HCPB TBM*, Fusion Eng. Des. **136** (2018) 1376, doi:10.1016/j.fusengdes.2018.05.014.

18 J Aubert *et al.*, *Status of the EU DEMO HCLL breeding blanket thermo-mechanical analyses*, Fusion Eng. Des. **109–111** (2016) 1655, doi:10.1016/j.fusengdes.2016.01.037.

19 M Abdou *et al.*, *Physics and technology considerations for the deuterium–tritium fuel cycle and conditions for tritium fuel self sufficiency*, Nucl. Fusion **61** (2021) 013001, doi:10.1088/1741-4326/abbf35.

20 M E Sawan and M A Abdou, *Physics and technology conditions for attaining tritium self-sufficiency for the DT fuel cycle*, Fusion Eng. Des. **81** (2006) 1131, doi:10.1016/j.fusengdes.2005.07.035.

21 M Abdou *et al.*, *Blanket/first wall challenges and required R&D on the pathway to DEMO*, Fusion Eng. Des. **100** (2015) 2, doi:10.1016/j.fusengdes.2015.07.021.

22 J E Menard *et al.*, *Fusion nuclear science facilities and pilot plants based on the spherical tokamak*, Nucl. Fusion **56** (2016) 106023, doi:10.1088/0029-5515/56/10/106023.

23 G Federici *et al.*, *Overview of the DEMO staged design approach in Europe*, Nucl. Fusion **59** (2019) 066013, doi:10.1088/1741-4326/ab1178.

24 U Fischer *et al.*, *Neutronics requirements for a DEMO fusion power plant*, Fusion Eng. Des. **98–99** (2015) 2134, doi:10.1016/j.fusengdes.2015.02.029.

25 M R Gilbert *et al.*, *Neutron-induced dpa, transmutations, gas production, and helium embrittlement of fusion materials*, J. Nucl. Mater. **442** (2013) S755, doi:10.1016/j.jnucmat.2013.03.085.

26 M Kovari *et al.*, *"PROCESS": A systems code for fusion power plants — Part 1: Physics*, Fusion Eng. Des. **89** (2014) 3054, doi:10.1016/j.fusengdes.2014.09.018.

27 R Kemp *et al.*, *Dealing with uncertainties in fusion power plant conceptual development*, Nucl. Fusion **57** (2017) 046024, doi:10.1088/1741-4326/aa5e2c.

28 J H You *et al.*, *Progress in the initial design activities for the European DEMO divertor: Subproject "Cassette"*, Fusion Eng. Des. **124** (2017) 364, doi:10.1016/j.fusengdes.2017.03.018.

29 P I Ford and G L Kulcinski, *From tritium consumer to breeding fleet: net blanket TBR and the cross-library case for multi-unit tritium export from a compact spherical-tokamak breeder*, Kronos Fusion Energy 2026 series, doi:10.5281/zenodo.22645706.

30 P I Ford and G L Kulcinski, *The tritium breeding ladder for a compact spherical-tokamak breeder: per-unit inventory, doubling time and the fleet path to tritium self-sufficiency*, Kronos Fusion Energy 2026 series, doi:10.5281/zenodo.22645746.

31 P I Ford, *Nuclear-data uncertainty quantification for tritium breeding: which 14 MeV cross-section channels set the error bar on the breeding ratio*, Kronos Fusion Energy 2026 series, doi:10.5281/zenodo.22645777.

32 P I Ford and G L Kulcinski, *Breeding-blanket and neutron-multiplier concept down-select for a compact spherical-tokamak breeder*, Kronos Fusion Energy 2026 series, doi:10.5281/zenodo.22645937.

33 P I Ford and G L Kulcinski, *CAD-faithful neutronics for a compact spherical-tokamak breeder: STEP-to-DAGMC Monte-Carlo transport reproducing the 3-D net tritium-breeding ratio*, Kronos Fusion Energy 2026 series, doi:10.5281/zenodo.22645881.

34 P I Ford and G L Kulcinski, *Component activation, waste-class routing, and decommissioning of a low-activation compact spherical-tokamak breeder*, Kronos Fusion Energy 2026 series, doi:10.5281/zenodo.22645846.

35 P I Ford, R J Weggel and C Weggel, *The consumable centrepost: coverage-versus-protection neutronics, coil integrity, and fused quench detection for a compact spherical-tokamak breeder*, Kronos Fusion Energy 2026 series, doi:10.5281/zenodo.22645704.

COLOPHON

How this document was made

The Kronos Fleet — Combined Editorial, 2026 is set in **Fraunces** (display), **Gelasio** (text), and **IBM Plex Mono** (data & equations), carried forward from the Kronos editorial design system.

The figures are rendered at 300 dpi from the deposited generator scripts; the document is composed as a single self-contained file with embedded fonts and imagery, paginated to US Letter, and rendered to PDF through a headless Chromium engine in matched light and dark editions.

Every headline quantity carries an evidence class; withdrawn and restated values are marked as such. Nothing herein is frozen beyond the founder-approved Tier-A set.

Explore it live — turn the interactive 3-D model, run the deposited solvers in the physics validator, and watch the companion film series.

LEGAL NOTICE

Notice, status, and distribution

Conceptual design & simulation study. This document reports a conceptual design and simulation study. It is not a construction commitment, a safety-analysis report, a regulatory filing, or an offer of securities. Forward-looking statements — schedules, costs, market sizes, and performance — are estimates subject to the limitations set out in the Simulations part and may change.

Numbers and their classes. Quantities are reported with evidence classes and case labels; modelled, assumed, and requirement-class values are identified as such and are not to be quoted without their labels.

Public edition. This edition carries the physics and design only; all financial, funding, and defense-commercial content has been removed for public distribution. The scientific text corresponds to the arXiv and journal submissions.

THE 2026 KRONOS SERIES

One programme, many papers

This editorial is one paper in the Kronos 2026 series — a real fusion company's complete, reproducible physics record for a spherical-tokamak breeder and its low-neutron D–^{3}He tandem-mirror burners. Every headline number is a frozen anchor in the Physics De-Risking Register.

Explore the whole programme: the De-Risking Register, the interactive 3-D model, and the physics validator.

KRONOS FUSION ENERGY

Beryllium and $Be_{12}Ti$ Neutron Multipliers for a Compact Spherical-Tokamak Breeder: Pebble Performance, Activation, and Closing Net TBR ≥ 1.05

A real fusion company building real machines. Explore the science, live.

Zenodo · doi:10.5281/zenodo.22645889

Read on kronosfusionenergy.com

The Physics De-Risking Register